Indian Journal of Engineering & Materials Sciences
Vol. 32, August 2025, pp. 493-501
DOI: 10.56042/ijems.v32i04.17709

Electrical discharge machining of EN-40B high carbon alloy steel: Investigation of recast layer and multi-performance optimization

Pratap Chandra Padhi[a], Nalamalapu Ravindra Reddy[a], Trupti Ranjan Mahapatra[b*], Punyapriya Mishra[b] & Somya Ranjan Parimanik[b]

[a]Central Institute of Petrochemicals Engineering and Technology (CIPET): IPT, Bhubaneswar 751 024, India
[b]Veer Surendra Sai University of Technology, Burla 768 018, India

Received:06 March 2025; accepted: 21 July 2025

This study has investigated the machinability of EN-40 high-carbon alloy steel in electrical discharge machining (EDM) by analyzing the recast layer morphology. Taguchi's L16 design and the desirability function approach (DFA) with a simple optimization algorithm (SOPTA) have been used to optimize pulse on time (Ton), pulse off time (Toff), low voltage current (LV), and high voltage current (HV). Performance metrics have included rate of material removal (RMR), tool wear rate (TWR), and surface roughness (Ra). The SOPTA algorithm using MATLAB 22a has determined the optimal settings (LV = 25A, HV = 2A, Ton = 40 µs, Toff = 25 µs) with a composite desirability of 0.5784. A confirmatory test has verified the optimal setting and compared it with the initial setting. The experimental results have shown that EDM performance has been significantly enhanced by the proposed method, with RMR, TWR, and Ra having improved by 66.32%, 70.36%, and 55.64%, respectively.

Keywords: Desirability function analysis, Electrical discharge machining, Recast layer, Simple optimization algorithm, Taguchi's methodology

1 Introduction

Electrical Discharge Machining (EDM) is a nontraditional process used for hard-to-machine conductive materials through high-intensity electrical discharges in a dielectric fluid[1]. Control factors, including tool materials, discharge current, pulse duration, and spark gap voltage, significantly influence machining efficiency, impacting rate of material removal (RMR), tool wear rate (TWR), surface roughness (Ra), cylindricity, circularity, and overcut[2]. Traditional (Taguchi methods, response surface methodology (RSM), Grey Relational Analysis (GRA), Technique for Order of Preference by Similarity to Ideal Solution (TOPSIS), Finite Element Analysis (FEA)) and contemporary (Genetic Algorithm (GA), Particle Swarm Optimization (PSO), artificial neural networks (ANNs), support vector machines (SVM)) techniques have been extensively applied for predictive modeling and process optimization to enhance EDM performance[3]. Empirical models have been developed to analyze key process parameters, indicating that discharge current and pulse-on time critically affect surface quality and RMR[4]. Surface modification techniques, such as carbon nanotube-coated electrodes, further improve machining precision[5]. Multi-objective optimization approaches like GRA, TOPSIS, and desirability function analysis have been employed to simultaneously optimize multiple responses, particularly in machining complex alloys like Inconel 625 and AISI 1045 steel[6-8]. Additionally, machine learning-based models aid in process optimization and predictive analytics, minimizing the need for extensive experimental trials[9]. Innovations in EDM include hybrid techniques such as powder-mixed dielectric fluids, ultrasonic-assisted EDM, and novel tool materials like Cu-Cr fabricated by powder metallurgy, which enhance machining efficiency and sustainability[10-12]. The use of artificial neural networks and metaheuristic algorithms, such as the SOPTA algorithm, further refines EDM process optimization[13-14]. Additionally, studies on the recast layer formation in micro-EDM contribute to understanding surface integrity improvements[15]. However, further advancements in analysis, modeling, and optimization are essential for EDM of unexplored materials to improve precision, efficiency, and sustainability in precision engineering industries.

We note that limited studies focus on optimizing process parameters for machining EN-40 high-carbon

*Corresponding author (E-mail: trmahapatra_pe@vssut.ac.in)

alloy steel using an electrolytic-grade copper electrode. This work aims to enhance the reliability and predictability of the EDM process by understanding its multiple interacting phenomena and analyzing the recast layer's morphology. The current experiments involve machining EN40B alloy steel in EDM, examining micro-scale surface characteristics using Energy Dispersive X-ray Spectroscopy (EDX) analysis conducted following Scanning Electron Microscopy (SEM). Additionally, a combined strategy of Taguchi's DOE and multiple optimization methods, including the desirability function approach (DFA) and a simple optimization algorithm (SOPTA), is employed to optimize the EDM process parameters for EN-40 alloy steel using a copper electrode.

2 Materials and Methods

The experiment is performed on a CNC-EDM (Model: MIC 432CS, ECOWIN, Taiwan) as shown in Fig. 1, using EN-40B alloy steel (Cr=3.25%, Si=0.89%, Mn=0.6%, Ni=0.4%, Mo=0.55%, C=0.38%, S=0.04%, P=0.035%, Fe=Balance) as the workpiece (90 mm × 50 mm × 10 mm) with properties: Density=7800 kg/m^3, 270 BHN, Tensile Strength=950 MPa, Yield stress=700 N/mm^2, Poisson's ratio=0.29. Thermal expansion= 10.4×10^{-6} per °C, Thermal Conductivity=23 W/m-K. Electrolytic-grade copper serves as the tool material and commercial-grade paraffin oil (freezing point: 94°C, specific gravity: 0.763) as dielectric fluid. Straight polarity and side flushing are applied, maintaining a constant flushing pressure of 10 psi. This study selects input variables based on pilot experiments and literature review, focusing on four controllable factors: low voltage current (LV), high voltage current (HV), pulse-off time (T_{off}), and pulse-on time (T_{on}). Their levels are determined by the machine's available parameter range, as shown in Table 1. The response variables include RMR (mm3/min), TWR (mm^3/min), and Ra (μm), with RMR and TWR calculated using Equations (1) and (2). Ra is measured using a Taylor Hobson Surtronic 3+ portable stylus profilometer, averaging three transverse readings from the machined surface.

Fig. 1 — CNC-EDM Machine (Model: MIC 432CS, ECOWIN, Taiwan).

$$MRR = \frac{1000 \times \Delta W_w}{\rho_w \times T} \quad \ldots(1)$$

$$TWR = \frac{1000 \times \Delta W_t}{\rho_t \times T} \quad \ldots(2)$$

where, ΔW_w and ΔW_t are the weight of material removed from the workpiece and tool during machining, ρ_w and ρ_t are the density of the workpiece and tool, and T is the machining time.

2.1 Taguchi's methodology

Taguchi's DOE utilizes an orthogonal array to minimize the number of trials while optimizing responses through signal-to-noise (S/N) ratio analysis. In EDM, where maximizing RMR and minimizing TWR and Ra are desired, S/N ratios are categorized as higher-is-better for RMR and smaller-is-better for TWR and Ra. These ratios are calculated using Equations (3) and (4) using the number of observations (n) and response values (r). The experiment follows a Taguchi L_{16} orthogonal array, designed using Minitab software with input levels from Table 1. The EDM-machined workpiece is shown in Fig. 2.

$$\frac{S}{N} = -10\log_{10}\frac{1}{n}\sum\frac{1}{r^2} \quad \ldots(3)$$

$$\frac{S}{N} = -10\log_{10}\frac{1}{n}\sum r^2 \quad \ldots(4)$$

2.2 SEM and EDX micrograph

The surface integrity of EDM-machined components is influenced by the recast layer, a thin resolidified

Table 1 — Level for various EDM parameters.

Parameters	Level 1	Level 2	Level 3	Level 4
LV (A)	10	15	20	25
HV (A)	0.5	1	1.5	2
T_{on} (μs)	10	20	30	40
T_{off} (μs)	10	15	20	25

Fig. 2 — Machined workpiece EN-40 alloy steel.

layer formed due to high heat and pressure during the process. The recast layer's thickness and microstructure impact the component's performance and reliability. SEM imaging provides detailed information on the layer's surface morphology, thickness, and any defects, while EDX analysis reveals the elemental composition of the recast layer, which differs from the bulk material due to intense heat and melting. Combined, SEM and EDX offer insights into the layer's microstructure and potential contamination, aiding in the optimization of EDM parameters and post-processing treatments. For microstructural analysis, a 5 mm-thick cross-section of the workpiece is polished progressively with silicon carbide emery papers of varying grit sizes (180, 300, 600, and 1000 μm), followed by mirror polishing with diamond pastes. The polished sample is then etched with Nital (2% nitric acid in methanol) to enhance contrast and reveal the microstructure. Micrographs are obtained using a JEOL SEM.

2.3 DFA-based SOPTA multi-objective optimization

Optimizing individual responses can lead to suboptimal results for other factors. Therefore, a combined approach using DFA and SOPTA is applied. DFA is a multi-response optimization method that converts a multi-objective problem into a single objective by assigning a desirability value (ranging from 0 to 1) to each response[13]. A value of 0 represents an unacceptable characteristic, while 1 indicates an optimal one. The overall desirability is calculated from these individual values, with the highest composite desirability indicating the optimal parameter settings[14]. The individual (d_i) and the overall (d_o) desirability indices are computed using experimentally obtained values (y_i), along with the maximum (y_{max}), minimum (y_{min}), and target (T) values[14].

$$d_i = \begin{cases} \text{Larger is better} & \text{Smaller is better} \\ 0,\ y_i \le y_{min}; & 1,\ y_i \le y_{min}; \\ \left(\frac{y_i - y_{min}}{y_{max} - y_{min}}\right)^r,\ y_{min} \le y_i \le y_{max}, r \ge 0; & \left(\frac{y_i - y_{max}}{y_{min} - y_{max}}\right)^r,\ y_{min} \le y_i \le y_{max}, r \ge 0; \\ 1,\ y_i \ge y_{min}; & 0,\ y_i \ge y_{min} \end{cases} \quad \ldots(5)$$

$$d_o = \left(d_1^{w_1} \times d_2^{w_2} \times \ldots\ldots \times d_i^{w_i}\right)^{1/w} \quad \ldots(6)$$

In each iteration of the SOPTA metaheuristic algorithm, solutions are explored and refined within a randomly generated population[13]. The exploration phase, guided by Equation (7), searches for improved solutions, while the exploitation phase, using Equation (8) with a reduced control parameter, fine-tunes results. The best solution from the previous iteration is used in both phases. If a new solution outperforms an existing one, it replaces it, and the process continues until the predefined iteration limit is reached.

$$X_{i,new} = X_{i,best} + C_1 \times R_i \quad \ldots(7)$$

$$X_{i,new} = X_{i,best} + C_2 \times R_i \quad \ldots(8)$$

Equations (7) and (8) in the algorithm differ only in their controlling parameters. Equation (7) uses parameter C1 (such that $1 \le C1 \le 2$), while Equation (8) uses parameter C2, which is half the value of C1. $X_{i,new}$ and $X_{i,best}$ represent the i^{th} parameters of the new solution and the best solution, respectively. R_i is a normally distributed random number with mean zero and standard deviation (σ_i), which is calculated from the i^{th} parameters of all population members. Initially, when solutions are widely dispersed, σ_i is larger, leading to greater variation in random numbers. As the search progresses and solutions converge, decreases, resulting in smaller random numbers and finer adjustments to new solutions. Unlike other algorithms, such as Particle Swarm Optimization (PSO), which uses random numbers within a fixed range [0, 1], SOPTA's random numbers vary with each iteration and parameter.

3 Results and Discussion

EDM experiments followed Taguchi's L16 orthogonal array, with Minitab software used for DOE and result analysis. ANOVA determined the significance of input parameters, and linear regression models optimized process settings. The goal was to

Table 2 — Taguchi's L16 orthogonal array design and output responses

Exp. Run	LV	HV	T_{on}	T_{off}	Responses			S/N ratio (dB)		
					RMR	TWR	R_a	RMR	TWR	R_a
	(A)		(μs)		(mm^3/min)		(μm)			
1	10	0.5	10	10	0.0605	0.0072	2.114	-24.3649	**42.8534**	**-6.5021**
2	10	1.0	20	15	0.0890	0.0098	2.379	-21.0122	40.1755	-7.5279
3	10	1.5	30	20	0.0920	0.0109	2.922	-20.7242	39.2515	-9.3136
4	10	2.0	40	25	0.1198	0.0112	3.817	-18.4309	39.0156	-11.6344
5	15	0.5	20	20	0.1489	0.0132	3.202	-16.5421	37.5885	-10.1084
6	15	1.0	10	25	0.0720	0.0108	2.133	-22.8534	39.3315	-6.5798
7	15	1.5	40	10	0.3890	0.0280	5.214	-8.2010	31.0568	-14.3434
8	15	2.0	30	15	0.2280	0.0214	3.629	-12.8413	33.3917	-11.1957
9	20	0.5	30	25	0.2030	0.0315	5.072	-13.8501	30.0338	-14.1036
10	20	1.0	40	20	0.3450	0.0340	5.917	-9.2436	29.3704	-15.4420
11	20	1.5	10	15	0.1920	0.0086	4.002	-14.3340	41.3100	-12.0455
12	20	2.0	20	10	0.2170	0.0159	4.493	-13.2708	35.9721	-13.0507
13	25	0.5	40	15	0.7010	0.0726	8.986	**-3.0856**	22.7813	-19.0713
14	25	1.5	30	10	0.6020	0.0690	7.760	-4.4081	23.2230	-17.7972
15	25	1.5	20	25	0.4219	0.0385	6.596	-7.4958	28.2908	-16.3856
16	25	2.0	10	20	0.3810	0.0360	5.814	-8.3815	28.8739	-15.2895

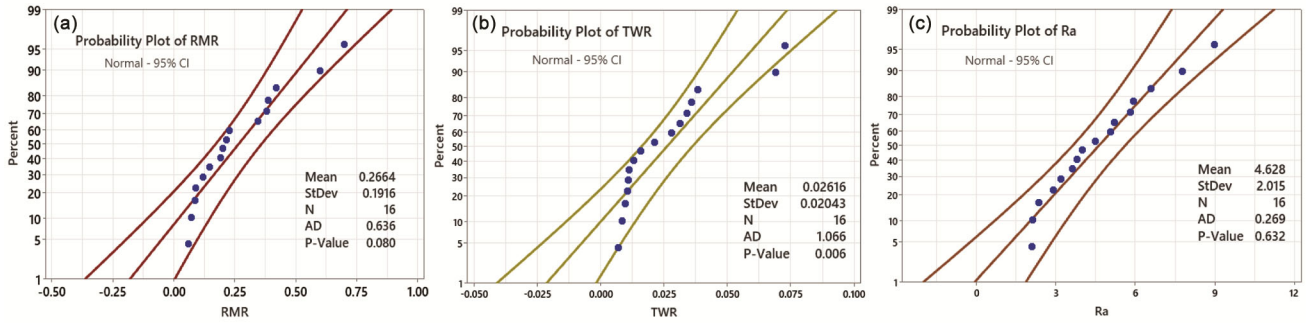

Fig. 3 — Normal probability plots for (a) RMR, (b) TWR, and (c) Ra

minimize TWR and Ra values and maximize RMR individually and simultaneously. Table 2 presents the experimental results, including S/N ratio values. Normal probability plots for RMR, TWR, and Ra (Fig. 3) indicate data alignment with a normal distribution, supported by p-values (>0.05) and Anderson-Darling statistics (RMR=0.636, TWR= 1.066, Ra=0.269). LV and Ton significantly influence all output responses, followed by HV and T_{off}, as shown in Table 3. RMR and TWR decrease with increasing HV, while Ra shows mixed behavior.

Table 4 presents ANOVA results, identifying significant factors affecting EDM responses. The analysis remains unbiased by scaling errors, constant bias, or response units. It includes DOF, SOS, SMS, F-value, and percentage contribution. LV current is the most influential factor, contributing 74.52% to RMR, 71.54% to TWR, and 76.37% to Ra, followed by T_{on} with 18.52%, 19.96%, and 21.9%, respectively. HV current and Toff have minimal impact, though T_{off} (6.13%) influences RMR, and HV current (6.03%) affects TWR. Error contributions are minimal at 0.047% (RMR), 0.208% (TWR), and 0.057% (Ra).

Table 5 summarizes the regression analysis and predictive equations to validate the accuracy of the fitted models. No response transformations were applied. The Pareto Chart of Standardized Effects for RMR, TWR, and Ra in Fig. 4 (a-c) further supports the ANOVA findings. High R^2 values (89.16% for RMR, 85.54% for TWR, and 94.49% for Ra) and adjusted R^2 values (85.22%, 80.28%, and 92.49%, respectively) confirm strong model fit and minimize regression errors.

3.1 Single response analysis using Taguchi's method

Figure 5 illustrates the main effect plots for RMR, TWR, and Ra, analyzing the impact of each input factor and identifying optimal parameter settings. A higher S/N ratio indicates minimal deviation from the desired output, ensuring better quality. For clarity, the highest S/N ratio values are highlighted. Based on

Table 3 — Response table for S/N ratios for responses.

Level/Parameter		1	2	3	4	Max-Min	Rank
RMR (higher-is-better)	LV	-21.133	-15.109	-12.675	-5.843	15.29	1
	HV	-14.461	-14.379	-12.689	-13.231	1.772	4
	T_{on}	-17.483	-14.580	-12.956	-9.740	7.743	2
	T_{off}	-12.561	-12.818	-13.723	-15.658	3.096	3
TWR (smaller-is-better)	LV	40.32	35.34	34.17	25.79	14.53	1
	HV	33.31	33.03	34.98	34.31	1.95	3
	T_{on}	38.09	35.51	31.48	30.56	7.54	2
	T_{off}	33.28	34.41	33.77	34.17	1.14	4
Ra (smaller-is-better)	LV	-8.745	-10.557	-13.66	-17.136	8.391	1
	HV	-12.446	-11.837	-13.022	-12.793	1.185	3
	T_{on}	-10.104	-11.768	-13.103	-15.123	5.019	2
	T_{off}	-12.923	-12.46	-12.538	-12.176	0.748	4

Table 4 — ANOVA for RMR, TWR, and Ra.

Response	Source	LV	HV	T_{on}	T_{off}	Error	Total
	DOF	3	3	3	3	3	15
RMR (higher-is-better)	SOS	0.410476	0.004823	0.102041	0.033428	0.000099	0.550867
	SMS	0.136825	0.001608	0.034014	0.011143	0.000033	-
	F	4163.6	48.92	1035.03	339.07	-	-
	Con.%	74.51454	0.875529	18.52371	6.068252	0.017972	100
TWR (smaller-is-better)	SOS	0.004477	0.00038	0.00125	0.000143	0.000013	0.00626
	SMS	0.001492	0.00013	0.00042	0.000048	0.000004	-
	F	352.19	29.64	98.26	11.21	-	-
	Con.%	71.54043	6.02429	19.9585	2.285075	0.20773	100
Ra (smaller-is-better)	SOS	46.5054	0.3682	13.3358	0.652	0.0349	60.8962
	SMS	15.5018	0.1227	4.4453	0.2173	0.0116	-
	F	1333.78	10.56	382.47	18.7	-	-
	Con.%	76.36831	0.60464	21.8992	1.070674	0.05731	100

Table 5 — Summary of Regression Analysis.

Response	S-value	R^2(%)	Adj R^2 (%)	Linear Regression Equation
RMR	0.0753938	89.16%	85.22%	$RMR = -0.205 + 0.02676 \times \text{LV} - 0.0258 \times HV + 0.00699 \times T_{on} - 0.00799 \times T_{off}$
TWR	0.0090714	85.54%	80.28%	$TWR = -0.022 + 0.002738 \times \text{LV} - 0.00788 \times HV + 0.000763 \times T_{on} - 0.000513 \times T_{off}$
Ra	0.552321	94.49%	92.49%	$R_a = -1.677 + 0.2954 \times \text{LV} - 0.216 \times HV + 0.0808 \times T_{on} - 0.0351 \times T_{off}$

the main effect analysis and response table, the optimal EDM process parameters are determined as: Maximum RMR: LV current = 25 A, HV current = 1.5 A, T_{on} = 40 µs, T_{off} = 10 µs; Minimum TWR: LV current = 10 A, HV current = 1.5 A, T_{on} = 10 µs, T_{off} = 15 µs; and Minimum Ra: LV current = 10 A, HV current = 1 A, T_{on} = 10 µs, T_{off} = 25 µs.

3.2 Recast layer analysis

EDM's thermal effects play a crucial role in determining surface characteristics. The recast layer forms due to the fusion of tool and workpiece materials, along with elements from the dielectric fluid, which solidify rapidly upon cooling. Reducing defects in this layer is essential for improving surface quality. Research indicates that peak current and applied voltage significantly impact recast layer formation, while Ton and Toff have a moderate influence[15]. To analyze these effects, SEM micrographs were taken at two parametric settings: (i) LV = 25 A, HV = 1.5 A, T_{on} = 40 µs, T_{off} = 10 µs, and

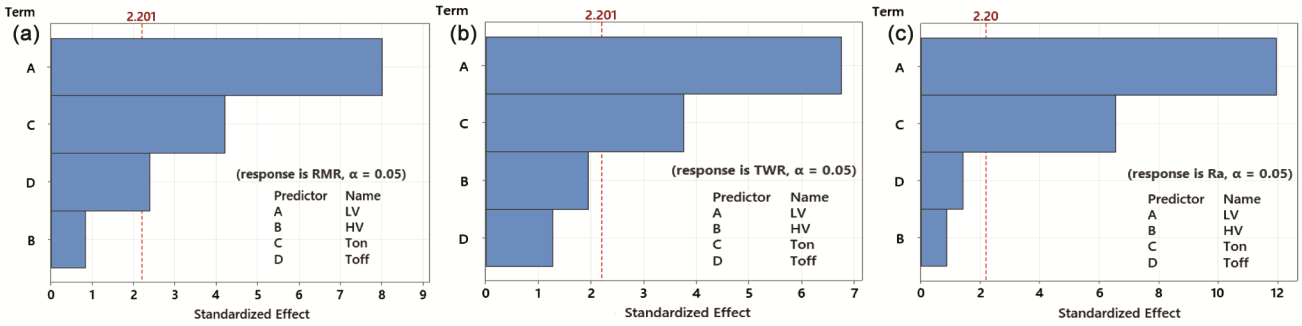

Fig. 4 — Pareto Charts for (a) RMR, (b) TWR, and (c) Ra

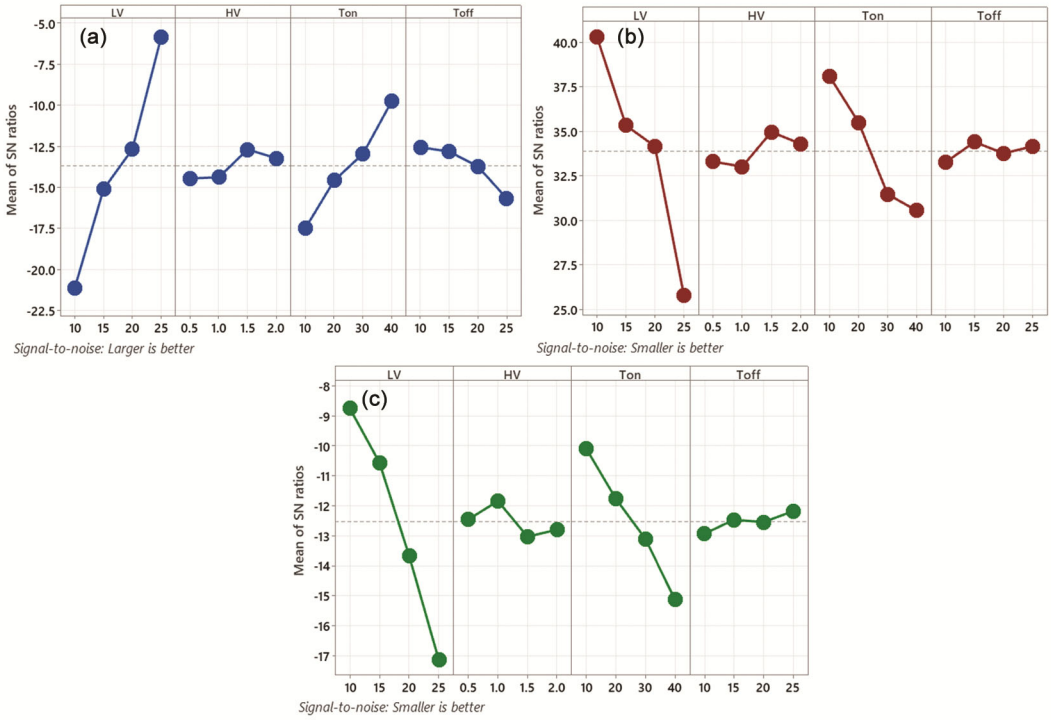

Fig. 5 — Main Effects Plot for SN ratios (a) RMR, (b) TWR, and (c) Ra

(ii) LV = 10 A, HV = 0.5 A, T_{on} = 10 µs, T_{off} = 10 µs. The machined surface appears mostly smooth (Fig. 6), but voids are more prevalent at higher LV currents due to gas entrapment. Cracks are observed at increased HV currents and longer pulse durations, likely caused by thermal stress from rapid cooling[15]. Additionally, spherical resolidified droplets indicate molten material expulsion and re-solidification on the surface. The cross-sectional view of the recast layer for the selected EDM parameters is shown in Fig. 7(a & b). An average recast layer thickness of 71 µm is observed on EN-40B high-carbon alloy steel. The micrograph reveals a pearlite microstructure with alternating ferrite and cementite lamellae on the workpiece surface. EDX analysis (Fig. 8) confirms elemental redistribution during EDM, showing carbon enrichment in the recast layer despite the Cr-rich base material. This occurs as carbon from the dielectric fluid interacts with the workpiece and tool materials, depositing on the machined surface[15].

3.3 Multi-performance optimization by DFA-based SOPTA

Using the DFA approach, all three responses are combined into a single d_c, with individual desirability values listed in Table 6. The higher-is-better criterion applies to RMR, while the lower-is-better criterion applies to TWR and Ra. A higher d_c indicates a closer match to the ideal response, enabling multi-response optimization through a single objective. For EDM of EN-40B steel, the optimal setting (LV = 15

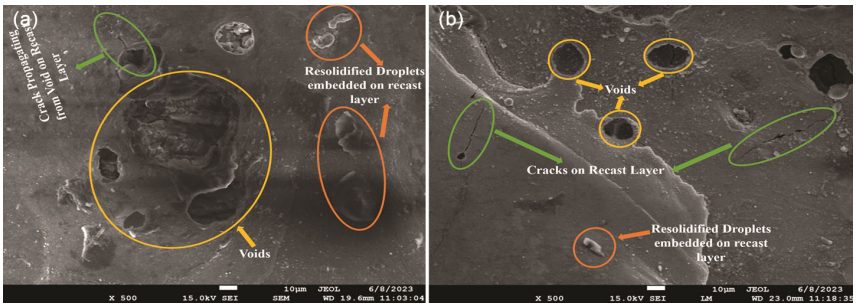

Fig. 6 — SEM image of surface morphology at (a) LV= 10A, HV= 0.5A, T_{on}=10µs, T_{off}=10µs and (b) LV= 10A, HV= 2A, T_{on}=20µs, T_{off}=15µs.

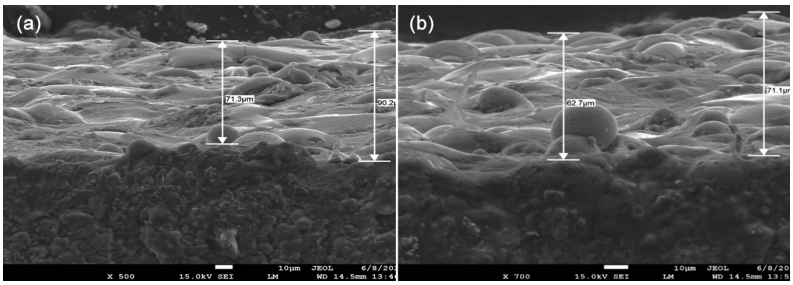

Fig. 7 — SEM image of the recast layer at (a) LV= 10 A, HV= 0.5A, T_{on}=10µs, T_{off}=10µs. and (b) LV= 10 A, HV= 2A, T_{on}=20µs, T_{off}=15µs.

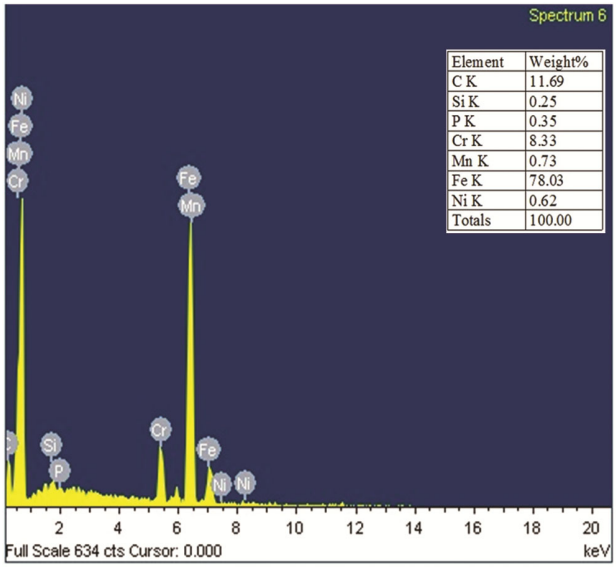

Fig. 8 — EDX of the machined surface.

A, HV = 1.5 A, T_{on} = 40 µs, T_{off} = 10 µs) is identified in experimental run 7, achieving the highest d_c (0.5728). Regression analysis generates the objective function (Equation 9) with R^2 = 89.6% and is optimized using SOPTA in MATLAB 22a. The final optimal parameter settings are in Table 7, and the SOPTA convergence curve is shown in Fig. 9.

Table 6 — Individual desirability and composite desirability.

Sl. No.	Individual Desirability			d_c	Rank
	d_i (RMR)	d_i (R_a)	d_i (TWR)		
1	0.0000	1.0000	1.0000	0.0000	15
2	0.0435	0.9614	0.9602	0.3428	11
3	0.0481	0.8824	0.9434	0.3424	12
4	0.0905	0.7522	0.9388	0.4001	10
5	0.1349	0.8417	0.9083	0.4693	7
6	0.0175	0.9972	0.9450	0.2551	13
7	0.5011	0.5489	0.6820	0.5728	1
8	0.2555	0.7795	0.7829	0.5386	2
9	0.2174	0.5696	0.6284	0.4273	9
10	0.4340	0.4466	0.5902	0.4858	6
11	0.2006	0.7253	0.9786	0.5225	3
12	0.2387	0.6538	0.8670	0.5138	4
13	1.0000	0.0000	0.0000	0.0000	15
14	0.8261	0.1784	0.0550	0.2013	14
15	0.5513	0.3478	0.5214	0.4645	8
16	0.4889	0.4616	0.5596	0.5021	5

Table 7 — Optimum parameters obtained from the SOPTA algorithm.

A: LV (A)	B: HV (A)	C: T_{on} (µs)	D: T_{off} (µs)	Optimum d_c
25	2	40	25	0.5784

3.4 Confirmation test

The confirmation test is crucial in experimental design to validate optimized settings and ensure prediction reliability. It bridges the gap between theoretical models and real-world performance. In this study, additional EDM experiments were conducted

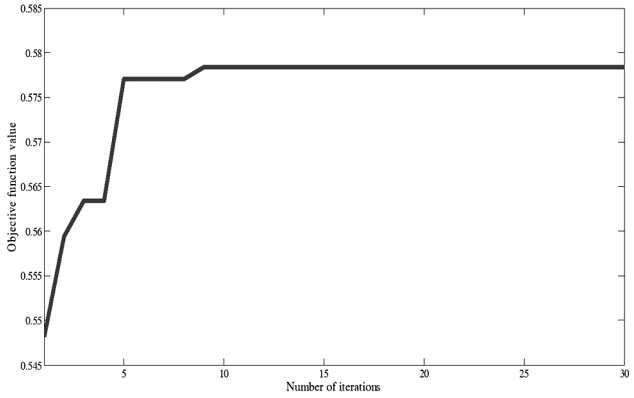

Fig. 9 — Convergence curve for the SOPTA.

using optimal parameters from Taguchi's method and DFA-based SOPTA to assess improvements in RMR, TWR, and Ra. For Taguchi's method, comparing predicted and actual responses confirmed accuracy, with results in Table 8 showing enhanced S/N ratios and response values. RMR increased by 0.8845% (0.0765 dB), while TWR and Ra decreased significantly by 46.94% (4.08 dB) and 27.25% (2.76 dB), respectively. For multi-response optimization, DFA-based SOPTA results showed a dc increase of 0.9777% over experimental run 7, with RMR, TWR, and Ra improving by 66.32%, 70.36%, and 55.64%, respectively. SEM analysis (Fig. 10a) revealed a thin recast layer (13.7–36.2 µm) with minimal defects.

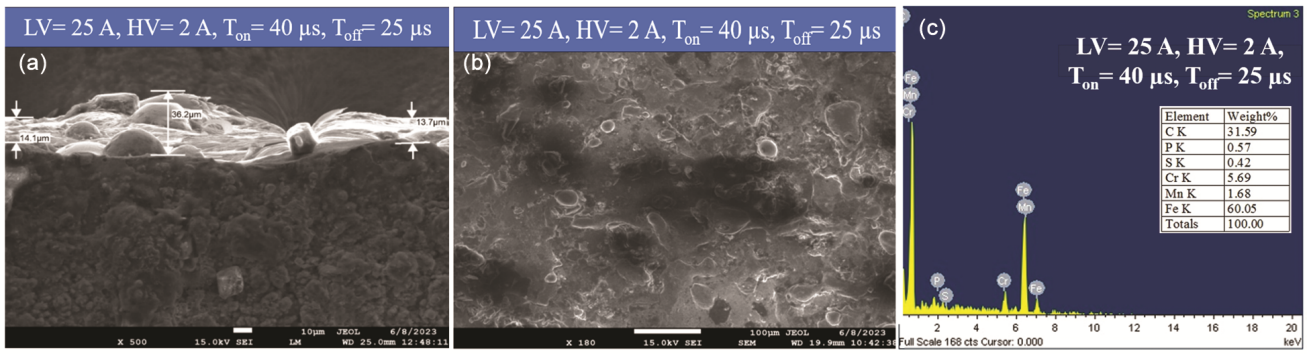

Fig. 10 — (a, b) SEM image of recast layer and (c) EDX of the machined surface.

Table 8 — Results of the Confirmation Experiment.

Method		Response	Process parameter (LV(A), HV(A), T_{on}(µs), T_{off}(µs)) Initial	Optimal Prediction	Optimal Experiment
Taguchi	RMR	Level	25, 0.5, 40, 15	25, 1.5, 40, 10	
		RMR (mm^3/min)	0.701	0.7069	0.7072
		Improvement (%)		0.8845	
		S/N Ratio (dB)	-3.0856	0.23691	-3.0091
		Improvement (dB)		0.0765	
	TWR	Level	10, 0.5, 10, 10	10, 1.5, 10, 15	
		TWR (mm^3/min)	0.0072	0.00346	0.0049
		Improvement (%)		46.9388	
		S/N Ratio (dB)	42.85335	46.08563	46.9357
		Improvement (dB)		4.0824	
	Ra	Level	10, 0.5, 10, 10	10, 1, 10, 25	
		R_a (µm)	2.114	1.39112	1.538
		Improvement (%)		37.4512	
		S/N Ratio (dB)	-6.5021	-5.288043	-3.73913
		Improvement (dB)		2.7630	
DFA-SOPTA		Level	15, 1.5, 40, 10	25, 2, 40, 25	
		RMR (mm^3/min)	0.389		0.647
		TWR (mm3/min)	0.028		0.0083
		R_a (µm)	5.214		2.313
		d_c	0.5728	0.5784	-
		Improvement (%)		0.9777	

Surface topology (Fig. 10b) showed no major cracks or voids, and EDX analysis (Fig. 10c) confirmed high carbon content in the recast layer.

4 Conclusion

SEM analysis reveals increased voids in the recast layer under higher LV current, while cracks appear with higher HV current and longer pulse duration. Spherical resolidified droplets are observed, with the recast layer averaging 71 µm, increasing Ra. EDX confirms elemental changes, showing carbon along with ferrite and cementite. ANOVA results indicate LV current as the most influential parameter, contributing 74.52% to RMR, 71.54% to TWR, and 76.37% to Ra, followed by Ton at 18.52%, 19.96%, and 21.9%, respectively. HV current and Toff have minimal effects. Optimal parameters from Taguchi analysis are LV=25 A, HV=1.5 A, T_{on}=40 µs, T_{off}=10 µs for RMR; LV=10 A, HV=1.5 A, T_{on}=10 µs, T_{off}=15 µs for TWR; and LV=10 A, HV=1 A, T_{on}=10 µs, T_{off}=25 µs for Ra. Multi-objective optimization using DFA-based SOPTA identified LV=25 A, HV=2 A, Ton=40 µs, and Toff=25 µs as the best combination, achieving 0.9777% improvement in composite desirability, with RMR, TWR, and Ra improving by 66.324%, 70.357%, and 55.639%, respectively. Confirmation tests validated 0.8845%, 46.9388%, and 27.2469% improvements in RMR, TWR, and Ra under optimal conditions.

References

1 Baroi B K, Jagadish J & Patowari P K, *J Braz Soc Mech Sci Eng*, 44(2) (2022) 59.

2 Singh V, Sharma A K, Goyal A, Saxena K K, Negi P & Rao P C S, *Adv Mater Process Technol*, 10(2) (2024) 517.

3 Matanda B K, Patel V, Singh B, Joshi U, Joshi A, Oza A D, Gupta M & Kumar S, *Int J Interact Des Manuf*, 18 (2024) 5343.

4 Chattopadhyay K D, Verma S, Satsangi P S & Sharma P C, *J Mater Process Technol*, 209(3) (2009) 1454.

5 Kumar S S, Varol T, Canakci A, Kumaran S T & Uthayakumar M, *Int J Lightweight Mater Manuf*, 4(1) (2021) 127.

6 Kar S K, Mishra P K, Sahu A K, Mahapatra S S & Thomas J, *Int J Interact Des Manuf*, 17(2) (2023) 931.

7 Hasan M M, Saleh T, Sophian A M, Rahman A, Huang T & Ali M S M, *Int J Adv Manuf Technol*, 127 (2023) 2125.

8 Singh R, Singh R P & Trehan R, *Sensors Int*, 3 (2022) 100179.

9 Faisal N & Kumar K, *Technologies*, 6(2) (2018) 54.

10 Harane P P, Wojciechowski S & Unune D R, *J Mater Res Technol*, 20 (2022) 2542.

11 Das M K, Kumar K, Barman T K & Sahoo P, *Int J Mach Machinability Mater*, 15(3–4) (2014) 235.

12 Shard A, Garg M P & Gupta V, *World J Eng*, 21(6) (2024) 1074.

13 Hasançebi O, Azad S K. *Int J Optim Civil Eng*, 2(4) (2012) 479.

14 Thomas J & Mahapatra S S, *Perspect Sci*, 8 (2016) 159.

15 Wang C, Wang H, Chu X, Lu Y & He H, *Materials*, 17(5) (2024) 1073.